Auto-aligning stimulated emission depletion microscope using adaptive optics

Travis J. Gould,[1,*] Emil B. Kromann,[2] Daniel Burke,[3] Martin J. Booth,[3,4,6] and Joerg Bewersdorf[1,2,5]

[1]*Department of Cell Biology, Yale School of Medicine, 333 Cedar Street, New Haven, Connecticut 06510, USA*

[2]*Department of Biomedical Engineering, Yale School of Medicine, 333 Cedar Street, New Haven, Connecticut 06510, USA*

[3]*Department of Engineering Science, University of Oxford, Parks Road, Oxford OX1 3PJ, UK*

[4]*Centre for Neural Circuits and Behaviour, University of Oxford, Mansfield Road, Oxford OX1 3SR, UK*

[5]*e-mail: joerg.bewersdorf@yale.edu*

[6]*e-mail: martin.booth@eng.ox.ac.uk*

**Corresponding author: travis.gould@yale.edu*

Received March 22, 2013; accepted April 17, 2013;
posted April 26, 2013 (Doc. ID 187651); published May 22, 2013

Stimulated emission depletion (STED) microscopy provides diffraction-unlimited resolution in fluorescence microscopy. Imaging at the nanoscale, however, requires precise alignment of the depletion and excitation laser foci of the STED microscope. We demonstrate here that adaptive optics can be implemented to automatically align STED and confocal images with a precision of 4.3 ± 2.3 nm. © 2013 Optical Society of America

OCIS codes: (070.6120) Spatial light modulators; (100.6640) Superresolution; (110.0180) Microscopy; (180.2520) Fluorescence microscopy.

http://dx.doi.org/10.1364/OL.38.001860

The advent of fluorescence nanoscopy has allowed biological imaging at spatial scales approaching the molecular level [1]. The diffraction barrier has been surpassed using either point-spread-function (PSF) engineering through the targeted switching of fluorophores or through precise localization of single fluorophores whose emission is stochastically switched on and off [2]. Of the former class of approaches, stimulated emission depletion (STED) microscopy [3] is the most common implementation. In STED microscopy, excited fluorophores are forced back to their electronic ground state by stimulated emission before they spontaneously fluoresce. This fluorescence-quenching transition is mediated by a so-called depletion laser whose wavelength is tuned to the red-shifted tail of the emission spectrum of the fluorophore. The focus of the depletion laser features a central intensity-zero that defines the subdiffraction region from which fluorescence may be emitted and collected. Optimal STED imaging therefore requires precise alignment of the intensity-zero of the STED focus to the center of the excitation focus. Conventionally, the relative alignment of the two laser foci has been achieved by imaging scattered laser light from gold beads and adjusting the position of one focus relative to the other until the PSFs align. However, this approach requires switching to a reflectance imaging mode and has typically relied on manual adjustment of the position of the foci. In this Letter, we present a novel automatic alignment approach for STED microscopy using adaptive optics, which allows relative spatial alignment of the depletion and excitation foci in all three dimensions. A key benefit of this method is that it uses feedback from the STED fluorescence images to ensure precise alignment of the two foci, thus avoiding any problems that arise from mismatch between reflection and fluorescence imaging modes.

Adaptive optics has previously been combined with STED microscopy by incorporating a spatial light modulator (SLM) in the depletion beam path [4]. This allows not only modulation of the phase profile to generate a STED focus [5,6], but also adaptive correction of the system- and sample-induced aberrations that reduce the beam quality and compromise resolution [4]. In this past study [4], adaptive correction of aberrations was achieved using a sensorless approach in which the quality of STED images was judged using a metric that accounts for both image brightness and resolution. Optimization of this metric permitted the indirect measurement (and hence correction) of aberrations. We demonstrate here that an SLM can also be used for automatic alignment of STED microscopes using a similar image-feedback loop. This approach determines the overlap of the depletion and excitation foci quantitatively based on an image quality metric, rather than on visual inspection or operator judgment. Though a STED microscope insensitive to drift has been proposed by coupling both beams into the same optical fiber [7], most STED systems rely on manual alignment, which can often limit the performance of these systems. With the approach presented here, manual positioning of laser foci is no longer required on a routine basis and the need for reflectance imaging capabilities is eliminated since fluorescent samples are used for the alignment procedure.

The experimental setup was similar to that reported previously [4]. In short, an SLM placed in the depletion beam path, conjugate to the objective back aperture, enables addition of the STED phase mask (helicoidal ramp or circular $\lambda/2$ step) and compensation for system-induced aberrations (Fig. 1).

Our new auto-alignment scheme was implemented by applying known amounts of tip or tilt (Zernike modes 2 and 3) to the SLM and then acquiring a STED image. The routine was performed by imaging 100 nm crimson beads (C47248, Invitrogen) attached to a no. 1.5 coverslip using poly-L-lysine and mounted in 97% thiodiethylene glycol. As discussed in the following, a suitable metric was used to measure the image quality of each STED image.

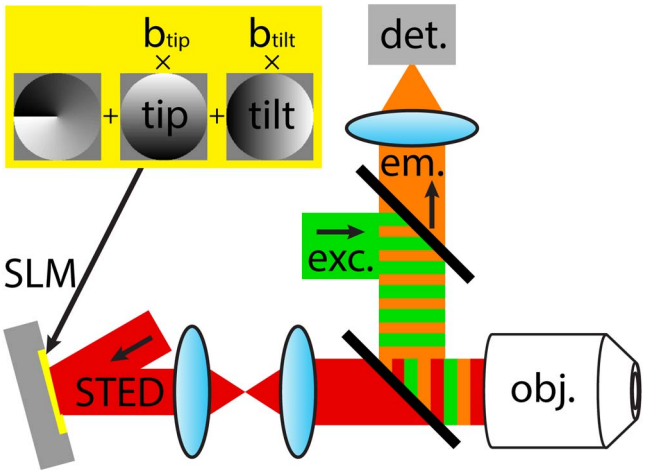

Fig. 1. Simplified schematic of the STED setup. The SLM displays a helicoidal phase ramp plus a sum of the Zernike polynomials tip and tilt weighted by the bias amplitudes b_{tip} and b_{tilt}. This phase pattern is imposed on the reflected STED laser and imaged into the pupil plane of the objective (obj.) Dichroic mirrors direct excitation light (exc.) onto the objective and emitted light (em.) onto the detector (det.). For 3D alignment, a circular $\lambda/2$ phase mask replaced the helicoidal phase ramp on the SLM, and a defocus term was included.

The STED images will be brightest when the position of the intensity-zero of the depletion focus is aligned to the center of the excitation focus. However, gross misalignment (lack of overlap) of the beams will result in conventional confocal images, which are typically even brighter than the STED images. Hence, simple optimization of image brightness cannot provide a reliable indication of alignment. Therefore, our alignment routine first performs a coarse adjustment using a metric that combines both image brightness and sharpness,

$$M = S - \beta B/(1 + \exp[-k(S - S_T)]), \tag{1}$$

where B and S are the brightness and sharpness metrics, respectively [4]. S_T is a threshold (typically 90% of the peak sharpness), and k and β are constants chosen empirically. The use of a sharpness measure ensures that applied corrections do not shift the depletion focus away from the excitation focus, which would result in a conventional confocal image. After each coarse correction using the metric defined in Eq. 1, a second iteration for fine alignment is performed over a smaller tip/tilt-amplitude range using only the image brightness as the image quality metric.

The procedure was first tested using a helicoidal phase mask that produces a toroidal depletion focus [8]. Figure 2(a) shows the initial misalignment between the excitation and STED foci (imaged using gold beads). Note that the gold bead images are shown for illustration purposes and were not necessary for the alignment routine, which relied solely on the STED fluorescence images. Figure 2(b) shows the corresponding overlay of a confocal and a STED image of 100 nm fluorescent beads in the same field of view. The line profile across a single bead [Fig. 2(c)] clearly reveals the misalignment of the depletion focus in both the x and y directions. The alignment routine was performed as described above

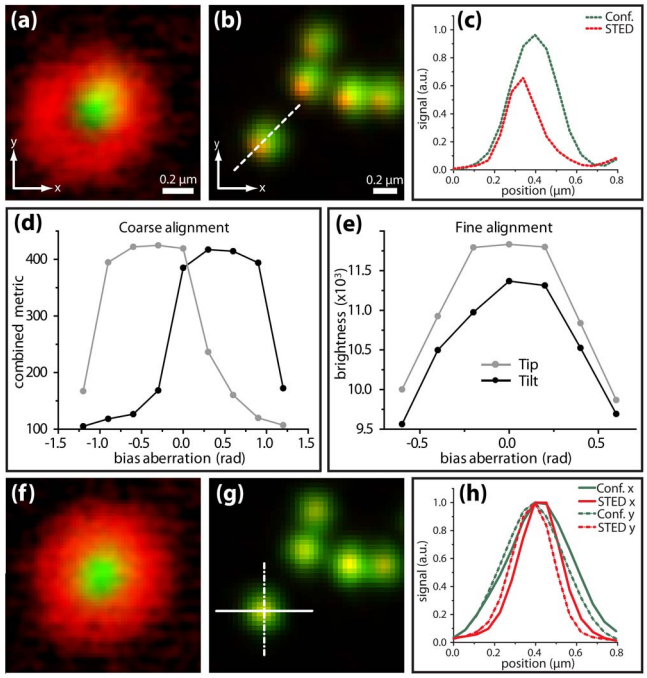

Fig. 2. Alignment of toroidal STED focus. (a) Merger of the excitation focus (green) and a poorly aligned depletion focus (red). (b) Merger of corresponding confocal (green) and STED (red) images of fluorescent beads imaged with the foci shown in (a). (c) Line profiles as indicated in (b): confocal (green) and STED (red). (d), (e) Metric curves for alignment procedure: (d) initial coarse alignment using metric defined in Eq. 1 and (e) subsequent fine adjustment optimized STED image brightness. (f)–(h) Same as (a)–(c) after running the auto-alignment routine. To demonstrate the increased STED image intensity in (h) relative to (c), the confocal and STED curves are normalized to their respective maximal values in (f). All images are smoothed using a Gaussian filter with a full width half-maximum of 2.35 pixels. Pixel sizes are (a), (f) 20 nm and (b), (g) 40 nm.

[Fig. 2(d) and Fig. 2(e)], and another set of images was then acquired [Fig. 2(f) and Fig. 2(g)]. The line profiles for a single bead from this set of images [Fig. 2(h)] show that the centers of the intensity distributions for the confocal and STED images are now well aligned in both directions. A major advantage of the improved alignment is the significant increase in brightness of the STED image [Fig. 2(c) and 2(h)].

To quantify the precision and verify the reproducibility of our alignment routine, we imaged 100 nm crimson beads first in confocal mode, then in STED mode, and finally in confocal mode again. We then estimated the center positions of the fluorescent beads by fitting 2D Gaussian distributions to the confocal bead images and 2D Lorentzian distributions to the STED bead images. To correct for sample drift between images, the position estimates from the confocal images taken before and after the STED image were averaged for each fluorescent bead. The displacements between confocal and STED positions were then averaged to determine the shift between the two imaging modes. To analyze image displacement, the alignment routine was performed four times with two sets of confocal-STED-confocal image sequences taken for each alignment (with 7–13 beads

analyzed in each image sequence). Averaging the results of the resulting eight data sets showed an average displacement of 4.3 ± 2.3 nm of the STED image relative to the confocal image. This value is well below the typical resolution of most STED microscopes. A preferred displacement direction was not observed during these measurements.

Alignment of a 3D STED microscope is more challenging, as it requires the correct overlap of the foci in all three dimensions. We extended the auto-alignment method to 3D by switching from the helicoidal phase ramp to a circular $\lambda/2$ phase mask to produce a 3D depletion focus [9]. Axial sections of fluorescent beads show an initial misalignment along the optical axis [Fig. 3(a)]. For this STED phase mask, the alignment routine was implemented by first optimizing the defocus (using Zernike mode 4 as a quadratic approximation to the spherical defocus mode of the high-NA system) of the depletion beam using the combined (coarse) metric from Eq. 1. Subsequent iterations were performed to align the beams in all three dimensions by maximizing only the brightness of the STED images. The resulting axial sections [Fig. 3(b)] and corresponding line profiles [Fig. 3(c)] show that the beams are now well aligned along the optical axis. Furthermore, the optimized alignment resulted in an ~18% increase in peak signal of the STED image. The resulting lateral alignment in the focal plane was comparable to the results obtained using the helicoidal phase ramp.

For the data shown here, seven images were acquired per iteration for each displacement mode. Though no significant photobleaching was observed for the fluorescent beads throughout these experiments, less photostable samples may require acquisition of fewer images or correction of the brightness metric to compensate for an exponential decrease in signal due to photobleaching. In principle only four images total are required to correct for tip, tilt, and defocus.

The auto-alignment routine takes advantage of the decoupled orthogonal effects for small displacements between the excitation and depletion foci. It should be noted that for larger misalignments, where sweeping the STED focus along a single axis would not result in any overlap of the two PSFs, a more sophisticated routine would be needed. Coarse adjustment could be implemented to move the STED focus to multiple positions in the imaging plane, effectively probing the quality metric in two dimensions, before determining the optimal tip and tilt amplitudes.

Using fluorescence image-based feedback, we have demonstrated the use of adaptive optics for automatic alignment of the depletion focus to the excitation focus in a STED microscope. As required for this type of microscopy, our method reliably attains an alignment precision on the nanometer scale. We expect this approach to significantly simplify the use of STED systems by eliminating the need for manual beam alignment. This routine can be easily performed as needed for a given experimental condition and is independent of the resolution of a particular STED system. Especially for two-color STED microscopy with different STED beams, our method has the potential to eliminate chromatic errors between the STED PSFs that can otherwise lead to co-localization artifacts [10]. Furthermore, this approach allows for precise switching between different STED phase masks that are well aligned to each other. Though demonstrated here using fluorescent beads, this approach should be amenable to any specimen.

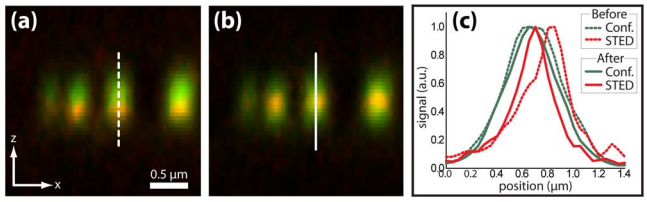

Fig. 3. Axial alignment of 3D STED focus. (a) Merge of confocal (green) and STED (red) images of fluorescent beads. (b) As in (a) after running the auto-aligning routine. (c) Line profiles as indicated in (a) and (b): confocal (green) and STED (red). All curves are normalized to their respective maximal values. The optimized STED peak was ~18% brighter than the nonaligned peak. Images shown in (a) and (b) were smoothed with a Gaussian filter with a 2 pixel (40 nm pixel size) full width half-maximum.

This work was supported by the Wellcome Trust (095927/A/11/Z, 095927/B/11/Z) and the Kavli Foundation. T.J.G. is supported by the National Institute of General Medical Sciences (F32GM096859). E.B.K. is supported by: The Denmark-America Foundation (Coloplast Stipend), Civilingeniør Frants Allings Legat, Knud Højgaards Fond, Reinholdt W. Jorcks Fond, Berg-Nielsens Legat, Ingeniør Alexandre Haynman og Hustru Nina Haynmans Fond, and Augustinus Fonden. M.J.B. was supported by the Engineering and Physical Sciences Research Council, UK (EP/E055818/1). J.B. discloses significant financial interest in Vutara Inc.

References

1. T. J. Gould, S. T. Hess, and J. Bewersdorf, Annu. Rev. Biomed. Eng. **14**, 231 (2012).
2. S. W. Hell, Nat. Methods **6**, 24 (2009).
3. S. W. Hell and J. Wichmann, Opt. Lett. **19**, 780 (1994).
4. T. J. Gould, D. Burke, J. Bewersdorf, and M. J. Booth, Opt. Express **20**, 20998 (2012).
5. E. Auksorius, B. R. Boruah, C. Dunsby, P. M. Lanigan, G. Kennedy, M. A. Neil, and P. M. French, Opt. Lett. **33**, 113 (2008).
6. G. Donnert, J. Keller, R. Medda, M. A. Andrei, S. O. Rizzoli, R. Luhrmann, R. Jahn, C. Eggeling, and S. W. Hell, Proc. Natl. Acad. Sci. U.S.A. **103**, 11440 (2006).
7. D. Wildanger, J. Buckers, V. Westphal, S. W. Hell, and L. Kastrup, Opt. Express **17**, 16100 (2009).
8. P. Torok and P. Munro, Opt. Express **12**, 3605 (2004).
9. T. A. Klar, S. Jakobs, M. Dyba, A. Egner, and S. W. Hell, Proc. Natl. Acad. Sci. USA **97**, 8206 (2000).
10. G. Donnert, J. Keller, C. A. Wurm, S. O. Rizzoli, V. Westphal, A. Schonle, R. Jahn, S. Jakobs, C. Eggeling, and S. W. Hell, Biophys. J. **92**, L67 (2007).